Time Domain Simulation of Helical Gyro-TWTs with Coupled Modes Method and 3D Particle Beam

Alexander Marek, Konstantinos A. Avramidis, Lukas Feuerstein, Stefan Illy, Manfred Thumm, *Life Fellow, IEEE,* Chuanren Wu and John Jelonnek, *Senior Member, IEEE*

***Abstract*— A new self-consistent time-domain model for the simulation of gyrotron traveling wave tubes with a helically corrugated interaction space (helical gyro-TWTs) is presented. The new model links classical methods, using the approach of slowly varying variables together with an expansion of the electromagnetic field in eigenmodes, and advanced full-wave PIC solvers. The aim is to significantly reduce the required calculation time compared to full-wave PIC solvers, while less strict assumptions are introduced as in the classical approaches of slowly varying variables. For the first time, the classical theory of coupled circular waveguide modes for the description of the operating electromagnetic eigenmode in the helical interaction space is combined with a 3D PIC representation of the electron beam. This allows the simulation of the beam-wave interaction over a broad bandwidth and at arbitrary harmonics of the cyclotron frequency. In addition, arbitrary electron beams (with spreads, offsets of the guiding center from the symmetry axis, etc.) can be investigated. The new approach is compared with the full-wave 3D PIC code CST Microwave Studio. A good agreement of the simulation results is achieved, while the computing time is significantly reduced.**

***Index Terms*— Gyrotron traveling wave tube (gyro-TWT), helically corrugated waveguide, coupled modes method, particle-in-cell (PIC).**

I. Introduction

NOVEL broadband high-power amplifiers at sub-THz frequencies are of considerable interest for future time-domain dynamic nuclear polarization (DNP) nuclear magnetic resonance (NMR) spectroscopy methods such as NOVEL [1] or TOP [2]. The development of those amplifiers is part of the current research. A promising candidate are gyrotron traveling wave tubes with a helically corrugated interaction space (helical gyro-TWTs) [3]. Helical gyro-TWTs can provide the required bandwidth and a high power at the same time.

In a gyro-amplifier, coherent electromagnetic radiation is amplified by a stimulated emission of bremsstrahlung from a beam of gyrating electrons. The simplest gyro-TWTs use a circular waveguide as circuit for the electron-wave interaction. In [3], an alternative type of gyrotron amplifier is proposed: a gyro-TWT with a helically corrugated waveguide as interaction region (HCIR). In the HCIR, the dispersion is radically changed for longitudinal wavenumbers close to zero. This allows a resonant electron-wave interaction over a significantly increased bandwidth. At the same time, the sensitivity to velocity spreads in the electron beam is reduced.

Besides the use as usual high-power amplifier, helical gyro-TWTs could be also used for the creation of innovative new types of microwave sources, such as in [4], where a broadband high-power helical gyro-TWT is coupled in a feedback loop with a saturable cyclotron absorber which enables the creation of powerful coherent ultra-short pulses. However, the simulation of such complex sources with 3D full-wave PIC simulation tools is very time consuming. An accurate and at the same time fast simulation tool would facilitate the development.

The approaches for the transient simulation of vacuum tubes can be split into two generic groups. The first group consists of Particle-In-Cell (PIC)-codes which usually include a 3D description of the particle motion and a full-wave simulation of the RF-field. The commercial software packages CST Microwave Studio [5] and MAGIC [6] belong to this group. Those programs are designed for universal application and can be used for the simulation of almost all types of vacuum electron tubes. Their disadvantage is the required high computing effort. Therefore, in the second group of programs, simplified physical models are used. Considering the simulation of gyro-devices, particularly classical gyrotron oscillators, the common codes are based on an eigenmode expansion of the electromagnetic field and the model of slowly varying variables. Several specialized programs exist for the simulation of gyrotron devices, e.g. [7]–[13].

While for the simulation of typical gyrotron devices with slowly varying circular interaction regions the coupling of discrete modes can be neglected, the helical corrugation provides an intentional coupling of particular modes. For sufficiently small corrugation amplitudes, this can be described by the coupled wave theory [14], [15] (based on the method of perturbation).

Based on the coupled wave theory, steady-state equations

Alexander Marek, Lukas Feuerstein, Stefan Illy, Manfred Thumm, Chuanren Wu and John Jelonnek are with the Institute for Pulsed Power and Microwave Technology (IHM), Karlsruhe Institute of Technology (KIT) Hermann-von-Helmholtz-Platz 1, 76344 Eggenstein-Leopoldshafen, Germany (e-mail: alexander.marek@kit.edu).

Konstantinos A. Avramidis was with IHM/KIT. He is now with the Department of Physics, National and Kapodistrian University of Athens, 15784 Zografou, Greece.

Manuscript received XXXX XX, XXXX; revised XXXX XX, XXXX.

were derived in the beginning of the theoretical analysis of helical gyro-TWTs [3]. The coupled system of equations for the wave and electrons was usually linearized [3], [15] which already allowed the analysis of different amplification regimes and the small-signal gain. For more complex cases, non-linear self-consistent steady-state equations were analyzed [16]. However, the analysis of transient phenomena, as for example required for the previously mentioned source of coherent pulses [4], is not possible with the averaged models. Therefore, the first time-domain model for the simulation of helical gyro-TWTs is presented in [17]. It uses transient coupled wave equations and the wave excitation is derived from differential equations for the electron transverse momentum. Two assumptions are made: (1) a sub-relativistic transverse electron velocity (relativistic effects are ignored); (2) the variation of the transversal momentum is slow compared to the high-frequency wave. Therefore, a slow transversal momentum can be introduced and allows the derivation of a non-isochronous oscillator equation for the slow transversal momentum [17].

In this paper, we present an alternative approach for the simulation of helical gyro-TWTs which does not require the mentioned assumptions on the electrons transverse momentum from [17]. The proposed approach can be seen as a hybrid between classical methods based on slowly varying variables and 3D full-wave PIC solvers. It combines a 3D PIC handling of the electron beam with the classical approach of slowly varying amplitudes and the coupled wave theory for the description of the electric field. The wave excitation by the electron beam is described with a source term derived from the arbitrary 3D beam of macro particles.

The proposed 3D electron beam provides a number of advantages: It allows a simple modeling and simulation of electron beams with arbitrary particle distributions (non-laminar beams, spreads, offset of the guiding center from the symmetry axis, etc.) and the consideration of inhomogeneities or misalignment of the static magnetic field is possible. Moreover, the general formulation of the source term allows an excitation of the field at arbitrary harmonics of the cyclotron resonance. In future, the individual handling of macro particles in the beam will enable the inclusion of additional physical effects such as influences of space-charge fields. Compared to full-wave PIC simulations, this model retains the significant gain of simulation speed and it still allows a detailed investigation and separation of the involved physical effects.

In this paper, the basic equations of the approach (section II) as well as the numerical solution of those equations are presented (section III). In section IV, the developed model is validated against the commercial full-wave PIC solver CST Microwave Studio [5] and a conclusion is drawn in section V.

II. Basic Equations

In a helical gyro-TWT, the beam-wave interaction takes place in a helically corrugated waveguide with an inner surface

$$r(\phi, z) = R + \tilde{r}\cos(\tilde{m}\phi - 2\pi z/\tilde{d}) \ , \tag{1}$$

where R is the waveguide mean radius; $\tilde{r}$, $\tilde{m}$ and $\tilde{k}_\parallel = 2\pi/\tilde{d}$ are the amplitude, azimuthal and axial number of the corrugation. Two rotating modes $\mathrm{TE}_{m_\mathrm{A},1}$ and $\mathrm{TE}_{m_\mathrm{B},1}$ are coupled with each other, if they fulfill the condition [14]

$$\tilde{m} = m_\mathrm{A} - m_\mathrm{B} \tag{2}$$

together with the Bragg resonance condition

$$\frac{2\pi}{\tilde{d}} \approx k_{\parallel\mathrm{A}} - k_{\parallel\mathrm{B}} \ , \tag{3}$$

where $k_{\parallel\mathrm{A}}$ and $k_{\parallel\mathrm{B}}$ are the axial wavenumbers of the two coupled modes A and B. In the following, three-fold helically corrugated waveguides ($\tilde{m} = 3$) are investigated exclusively.

For an optimal stability and broadband behavior of the helical gyro-TWT, the parameters of the three-fold helical corrugation are chosen such that the two partial waves of lowest order, namely the $\mathrm{TE}_{2,1}$ and $\mathrm{TE}_{1,1}$ modes, of a regular waveguide are coupled. From the coupling condition (2) with $\tilde{m} = 3$ it follows that this coupling is only possible if mode B is a counter-rotating $\mathrm{TE}_{-1,1}$ mode.

For a suppression of higher-order parasitic modes, the radius R is set such that the $\mathrm{TE}_{2,1}$ mode, which is co-rotating with the electrons, is near to cut-off at the operation frequency band and the cut-off frequency of the $\mathrm{TE}_{1,1}$ mode is far below the operating frequency. Therefore, the Bragg resonance condition (3) simplifies to:

$$\begin{aligned} k_{\parallel\mathrm{A}} &\approx 0 \ , \\ k_{\parallel\mathrm{B}} &\approx k \ , \\ \Rightarrow \frac{2\pi}{\tilde{d}} = \tilde{k}_\parallel &\approx k_{\parallel\mathrm{B}} \ , \end{aligned} \tag{4}$$

where k is the free-space wavenumber. As a consequence of the Bragg resonance condition (4), the coupling occurs between the first spatial harmonic of mode B (axial wavenumber shifted by $\tilde{k}_\parallel$) and the fundamental mode A.

In Fig. 1, the resulting dispersion curve for the helical eigenmode is shown together with the cyclotron resonance condition for the beam-wave interaction. Around zero axial wavenumber, the helical eigenmode has a nearly constant group velocity over a broad frequency band. As a result, it can be matched to resonantly interact with a gyrating electron beam over a broad bandwidth. A further benefit of the helical eigenmode is its ability to resonantly interact with an axis encircling electron beam (so-called large orbit beam) at the second cyclotron harmonic. This reduces the required magnetic field by a factor of 2, which is particularly advantageous at frequencies in the sub-THz range.

A. Wave Equation

The wave equations are simplified by the classical slowly varying amplitudes approximation [18]. For this, the electric field is expanded into orthogonal eigenmodes and a baseband transformation to a carrier frequency ω_0, which should be close to the expected operation frequencies, is performed. As a consequence, the electric field in the helically corrugated waveguide at the operation frequency band can be presented by the two partial waves

$$\boldsymbol{E}_\mathrm{A}(t, r, \phi, z) = \mathrm{Re}\left\{ A(t, z)\, \mathrm{e}^{\,j\omega_0 t}\, \hat{\boldsymbol{e}}_\mathrm{A}(r, \phi) \right\} \ , \tag{5}$$

$$\boldsymbol{E}_\mathrm{B}(t, r, \phi, z) = \mathrm{Re}\left\{ B(t, z)\, \mathrm{e}^{\,j\left(\omega_0 t - \tilde{k}_\parallel z\right)}\, \hat{\boldsymbol{e}}_\mathrm{B}(r, \phi) \right\} \ , \tag{6}$$

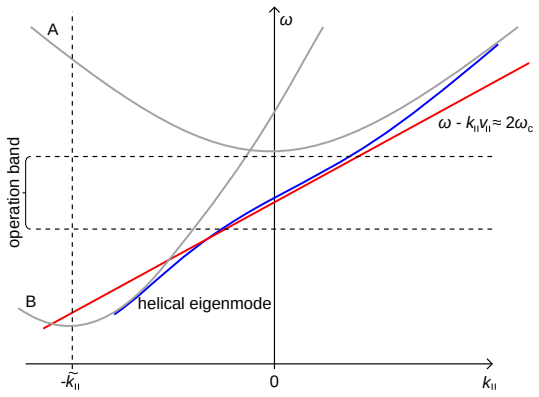

Fig. 1. Schematic dispersion diagram showing the partial waves coupled by the helical corrugation, the operating eigenmode of the helical waveguide, and the cyclotron resonance condition for an interaction at the second harmonic.

where j is the imaginary unit, A and B are the amplitudes and $\hat{\boldsymbol{e}}_{\mathrm{A,B}}$ are the transversal structures of the circular waveguide eigenmodes A and B (the expressions can be found, e.g. in [19]).

Setting the carrier frequency ω_0 to the cutoff frequency of mode A, the change of the complex wave envelope $A(t,z)$ can be assumed as slow compared to the phase term $\mathrm{e}^{\,j\omega_0 t}$. Consequently, the 1D Helmholtz equation for mode A can be approximated as [18]

$$\begin{aligned}&\frac{\partial^2 A}{\partial z^2}+k_{0\|}^2 A-j\frac{2k_0^2}{\omega_0}\frac{\partial A}{\partial t}\\ &=\underbrace{-\mu_0\,\mathrm{e}^{\,-j\omega_0 t}\iint\limits_{S_\perp}\frac{\partial \boldsymbol{J}}{\partial t}\cdot\hat{\boldsymbol{e}}_{\mathrm{A}}^{*}\,\mathrm{d}S_\perp}_{=S_{\mathrm{A}}}\ .\end{aligned}\tag{7}$$

The term S_{A} is called source term and describes an excitation of the field by an external source, e.g. the electron beam. A derivation of a source term for an arbitrary 3D particle beam is presented in the following section.

Since mode B is a traveling mode, operated far away from cut-off, the group velocity of the mode is almost constant for the operation frequency band. Therefore, the 1D Helmholtz equation can be further simplified compared to (7) by neglecting dispersion effects:

$$\begin{aligned}&\tilde{k}_\|\frac{\partial B}{\partial z}+\frac{k_0}{c_0}\frac{\partial B}{\partial t}-\frac{j}{2}\left(k_{0\|}^2-\tilde{k}_\|^2\right)B\\ &=\underbrace{\frac{j}{2}\,(-\mu_0)\,\mathrm{e}^{\,-j(\omega_0 t-\tilde{k}_\| z)}\iint\limits_{S_\perp}\frac{\partial \boldsymbol{J}}{\partial t}\cdot\hat{\boldsymbol{e}}_{\mathrm{B}}^{*}\,\mathrm{d}S_\perp}_{=S_{\mathrm{B}}}\ .\end{aligned}\tag{8}$$

Finally, a set of two coupled equations describing the eigenwave in a helically corrugated waveguide can be formulated:

$$\frac{\partial^2 A}{\partial z^2}-j2\frac{k_0}{c_0}\frac{\partial A}{\partial t}+k_{0\|\mathrm{A}}^2 A=S_{\mathrm{A}}+C_{\mathrm{B,A}}B\,,\tag{9}$$

$$\tilde{k}_\|\frac{\partial B}{\partial z}+\frac{k_0}{c_0}\frac{\partial B}{\partial t}-\frac{j}{2}\left(k_{0\|\mathrm{B}}^2-\tilde{k}_\|^2\right)B=\frac{j}{2}C_{\mathrm{A,B}}A\ .\tag{10}$$

Here, $C_{\mathrm{A,B}}$ and $C_{\mathrm{B,A}}$ are the coupling factors for the coupling of mode A to mode B and vice versa. The expressions are given in [15].

In (10), it is already taken into account that in a helical gyro-TWT a large orbit electron beam is typically used to enhance the mode selection and to prevent the excitation of parasitics. Such an electron beam excites only resonant modes with the azimuthal indices equal to the electron cyclotron harmonic number s. As a consequence, S_{B} can be omitted in (10). However, if a misaligned electron beam or a beam with strong spreads should be investigated, S_{B} must be taken into account.

B. Source Term

While it is common in the most approaches for the simulation of gyrotron devices to simplify the source term S by the Graf's addition theorem [20], here, the source term is directly evaluated for an arbitrarily moving particle and an arbitrary eigenmode $\hat{e}$. In the following, a brief overview of the derivation of this 'full' source term is given.

In (7) and (8), the source term is defined as the time derivative of a current density $\boldsymbol{J}$, integrated over the cross section of the waveguide:

$$S=\mu_0\iint\limits_{S_\perp}\frac{\partial \boldsymbol{J}}{\partial t}\cdot\hat{\boldsymbol{e}}^{*}\ \mathrm{e}^{\,-j\omega_0 t}\,\mathrm{d}S_\perp\ .\tag{11}$$

For a sum of point particles with position $\boldsymbol{r}_i$, velocity $\boldsymbol{v}_i$ and electric charge q_i, the electric current density can be expressed as

$$\boldsymbol{J}=\sum_i q_i\delta(\boldsymbol{r}-\boldsymbol{r}_i)\boldsymbol{v}_i\ ,\tag{12}$$

where $\delta(\boldsymbol{r}-\boldsymbol{r}_i)$ is the 3D delta function. After applying the definition of the delta function in cylindrical coordinates to (11), multiple applications of the chain rule and an integration over the waveguide cross-section $S_\perp$, the source term S_i of a single particle i calculates as:

$$\begin{aligned}S_i=\mu_0 q_i\mathrm{e}^{\,-j\omega_0 t}\Big[&-\delta'(z-z_i)\dot{z}_i\boldsymbol{v}_i\cdot\hat{\boldsymbol{e}}^{*}(r_i,\phi_i)\\&+\delta(z-z_i)\dot{\boldsymbol{v}}_i\cdot\hat{\boldsymbol{e}}^{*}(r_i,\phi_i)\\&+\delta(z-z_i)\dot{r}_i\boldsymbol{v}_i\cdot\left.\frac{\partial\hat{\boldsymbol{e}}^{*}(r,\phi_i)}{\partial r}\right|_{r=r_i}\\&+\delta(z-z_i)\dot{\phi}_i\boldsymbol{v}_i\cdot\left.\frac{\partial\hat{\boldsymbol{e}}^{*}(r_i,\phi)}{\partial\phi}\right|_{\phi=\phi_i}\Big]\ .\end{aligned}\tag{13}$$

Here, the dot on variables represents the time derivative $\frac{\partial}{\partial t}$.

It is worth emphasizing that no assumptions about the electron beam, the waveguide, the eigenmode or the cyclotron-harmonic are made. Therefore, (13) can be applied for arbitrary electric fields and waveguides which allows an extension of the developed program for future applications. Moreover, this source term is valid for interactions at all cyclotron harmonics.

III. Numerical Solution

For the numerical solution, a finite difference (FD) scheme is used. The time domain as well as the spatial domain of interest are discretized into N_t time steps of length Δt and N_z space steps of length Δz. For the calculation of a new time step $t+\Delta t$, first the field equations (9) and (10) are

solved. New particles are injected in every time step and with the known amplitude distribution of the waveguide modes along the interaction space, the particle positions are updated (particle pushing). Particles which leave the simulation space are killed after every particle pushing step. If additional effects such as space-charge fields or beam neutralization should be considered, their calculation can be introduced before the particle pushing. Finally, the source terms S_i are calculated with the known wave amplitudes and the updated particle positions and velocities. With the updated source terms, the field equations including the excitation by the electron beam can be solved in the next time step.

A. Coupled Wave Equations of a HCIR

For the numerical solution of the field equations, the implicit finite difference Crank-Nicolson scheme [21] is used which is of second-order, both in time and space. In the Crank-Nicolson scheme, the explicit first order forward finite difference for time step t and the implicit first order backward finite difference for time step $t+\Delta t$ are combined for a discretization of the time derivatives. For the spatial derivatives, a central difference scheme of second order is used. This gives the following discretization which can be applied to the field equations (9) and (10):

$$A = \frac{1}{2}\left(A_z^{t+1} + A_z^t\right) \tag{14}$$

$$\frac{\partial A}{\partial t} = \frac{A_z^{t+1} - A_z^t}{\Delta t} \tag{15}$$

$$\frac{\partial A}{\partial z} = \frac{1}{2}\left(\frac{A_{z+1}^{t+1} - A_{z-1}^{t+1}}{2\Delta z} + \frac{A_{z+1}^{t} - A_{z-1}^{t}}{2\Delta z}\right) \tag{16}$$

$$\frac{\partial^2 A}{\partial z^2} = \frac{1}{2}\left(\frac{A_{z+1}^{t+1} - 2A_{z}^{t+1} + A_{z-1}^{t+1}}{\Delta z^2} + \frac{A_{z+1}^{t} - 2A_{z}^{t} + A_{z-1}^{t}}{\Delta z^2}\right) \tag{17}$$

After a discretization of the equations (9) and (10) following the Crank-Nicolson scheme (14)-(17), a coupled system of linear equations

$$\underline{D_\mathrm{B}}\boldsymbol{B} + \underline{T_\mathrm{A}}\boldsymbol{A} = \boldsymbol{V}_\mathrm{A} \tag{18}$$

$$\underline{T_\mathrm{B}}\boldsymbol{B} + \underline{D_\mathrm{A}}\boldsymbol{A} = \boldsymbol{V}_\mathrm{B} \tag{19}$$

is derived, where $\underline{D_{\mathrm{A,B}}}$ represent $(N_z)\times(N_z)$ diagonal matrices and $\underline{T_{\mathrm{A,B}}}$ represent $(N_z)\times(N_z)$ tridiagonal matrices. The coupled equations can be rewritten as a single system of linear equations

$$\begin{pmatrix} \underline{D_\mathrm{B}} & \underline{T_\mathrm{A}} \\ \underline{T_\mathrm{B}} & \underline{D_\mathrm{A}} \end{pmatrix} \begin{pmatrix} \boldsymbol{B} \\ \boldsymbol{A} \end{pmatrix} = \begin{pmatrix} \boldsymbol{V}_\mathrm{A} \\ \boldsymbol{V}_\mathrm{B} \end{pmatrix} \tag{20}$$

which can be efficiently solved by the 'Schur-Complement' method:

$$\underline{G} = \underline{D_\mathrm{A}} - \underline{T_\mathrm{B}}\,\underline{D_\mathrm{B}^{-1}}\,\underline{T_\mathrm{A}} \tag{21}$$

$$\Rightarrow \underline{G}\boldsymbol{A} = \boldsymbol{V}_\mathrm{B} - \underline{T_\mathrm{B}}\,\underline{D_\mathrm{B}^{-1}}\boldsymbol{V}_\mathrm{A} \tag{22}$$

$$\Rightarrow \boldsymbol{B} = \underline{D_\mathrm{B}^{-1}}\boldsymbol{V}_\mathrm{A} - \underline{D_\mathrm{B}^{-1}}\,\underline{T_\mathrm{A}}\boldsymbol{A}\ . \tag{23}$$

With this method, the original problem of a $(2N_z)\times(2N_z)$ system of equation is reduced to a $(N_z)\times(N_z)$ system of equations (22) and a simple back-substitution (23). In the given case, this is possible because the inverse $\underline{D_\mathrm{B}^{-1}}$ for a diagonal matrix can be easily found.

The so-called Schur complement $\underline{G}$ is a penta-diagonal matrix. For a solution of the resulting system of linear equations, optimized algorithms are available, for example the `zgbtrs` function in the LAPACK [22].

It should be mentioned that the described method is only valid, as long as all of the diagonal elements of $\underline{D_\mathrm{B}}$ are non-zero. In the given problem, this corresponds to a non-zero coupling coefficient C in the equations (9) and (10). This is fulfilled for all helically corrugated waveguides. For very small or very large elements in $\underline{D_\mathrm{B}}$, this method becomes numerical unstable (bad conditioned matrix). However, for typical coupling coefficients in helical gyro-TWTs and for floating point types in double precision, we observed that the method remains numerically stable.

B. Source Term and Equations of Motion

The contributions of the particles to the source term are calculated with equation (13). For the spacial interpolation from the particle position to the amplitude nodes, the Dirac distribution $\delta(z)$ and it's derivative $\delta'(z)$ must be numerically evaluated. Because the amplitude nodes are equally distributed along the z axis with step-width Δz, $\delta(z)$ can be approximated by a one-variable function $\Phi(x)$ that scales with the step-width in the following manner:

$$\delta(z) \to \frac{1}{\Delta z}\Phi\left(\frac{z}{\Delta z}\right) = \frac{1}{\Delta z}\Phi(\hat{z}) \quad \text{with} \quad \hat{z} \equiv \frac{z}{\Delta z}\ , \tag{24}$$

$$\delta'(z) \to \frac{1}{\Delta z^2}\Phi'(\hat{z})\ . \tag{25}$$

For the function $\Phi(\hat{z})$, the cosine-approximation is used (a detailed derivation can be found in [23]). It allows a fast numerical evaluation and has a continuous derivative:

$$\Phi(\hat{z}) = \begin{cases} \frac{1}{4}\left(1+\cos\frac{\pi\hat{z}}{2}\right), & |\hat{z}| \le 2 \\ 0, & \text{otherwise} \end{cases} \tag{26}$$

$$\Phi'(\hat{z}) = \begin{cases} \frac{-1}{8}\sin\frac{\pi\hat{z}}{2}, & |\hat{z}| \le 2 \\ 0, & \text{otherwise}\ . \end{cases} \tag{27}$$

After the electromagnetic field is known (solution of the field equations from the first step and the optional additional fields such as space-charge fields), the particle positions and velocities are updated. This is done by solving the Lorentz equation

$$\frac{\mathrm{d}\boldsymbol{p}}{\mathrm{d}t} = q\left(\boldsymbol{E} + \boldsymbol{v}\times\boldsymbol{B}\right)\ , \tag{28}$$

where $\boldsymbol{p}$, $\boldsymbol{v}$ and q are the relativistic momentum, the velocity and the charge of a particle. $\boldsymbol{E}$ and $\boldsymbol{B}$ are the electric and magnetic fields. For the integration of (28), various particle integrators (particle pushers) have already been developed [24]. The most of these algorithms are suitable for the given propose. So far, the developed tool was successfully tested with an explicit fourth-order Runge-Kutta method [25] and the well known Boris algorithm [26].

In the proposed algorithm, the time step length Δt is determined by the particle pushing step. To allow an accurate

sampling of the gyration of the electrons, time steps between $\frac{2\pi}{50\omega_\mathrm{H}}$ and $\frac{2\pi}{100\omega_\mathrm{H}}$ have shown good results with the Boris and the Runge-Kutta method. If additional effects such as space-charge are included, a smaller time-step may be required.

The required spatial resolution Δz is determined by the solution of the wave amplitudes. An accurate sampling of the spacial phase change of the slow wave has been shown crucial and therefore a Δz of smaller than $\frac{1}{360(k_0-\tilde{k}_\parallel)}$ should be used.

IV. Comparison with Full-Wave PIC Simulations

The algorithm presented above is implemented in an object-oriented framework with the programming language C++. One advantage of the PIC approach is its excellent suitability for a solution in parallel. Therefore, the developed implementation utilizes parallelization on multi-core central processing units (CPUs). In the following, our implementation will be referred to as 'simpleRick'.

For the validation of the proposed approach, simulations are performed and compared with the commercial full-wave PIC tool CST Microwave Studio [5]. Two different setups are investigated: a W-band helical gyro-TWT for radar and communication applications with a center frequency of 94 GHz and a sub-THz gyro-TWT for spectroscopy applications around 263 GHz. For both setups, the gain at saturated output power for different frequencies is compared. To avoid the requirement of many time consuming simulations with different input-signal frequencies, a frequency-chirped signal with sufficient power is used as input for the time-domain simulations. In a post-processing step, the resulting frequency-modulated output signal is transformed to frequency-domain and the gain for different frequencies is calculated.

A. W-Band Helical Gyro-TWT

The W-band gyro-TWT has a three-fold helical interaction region with $R = 1.45\,\mathrm{mm}$, $\tilde{r} = 0.23\,\mathrm{mm}$, $\tilde{d} = 3.2\,\mathrm{mm}$ and a length of $L = 35\,\tilde{d}$. It is operated with an electron beam current of 1.5 A, a beam voltage of $U_\mathrm{b} = 50\,\mathrm{kV}$ and a pitch factor of $\alpha = v_\perp / v_\parallel = 1.0$ at a constant magnetic field of 1.82 T.

For the CST MS simulation model, a spatial discretization of $dx = dy = 0.025\lambda$ in the transversal dimension and $dz = 0.03\lambda$ in the longitudinal dimension is used which results in $4 \cdot 10^6$ mesh cells. While in [27] an even finer discretization is recommended, the chosen values have shown a good compromise between accuracy and calculation time. The electron beam is modeled by $200 \cdot 10^3$ macro particles.

In the simpleRick setup, a spacial discretization of $dz = 0.01\lambda$ is used. The number of macro particles is chosen similarly to the CST MS simulation to allow a good comparability. The used time steps of around 0.15 ps are also chosen similarly for both simulation tools.

For CST MS, the simulation takes 5:30 h on a desktop computer with a 12 core AMD Ryzen™ 9 5900X CPU. In comparison, the simulation with simpleRick takes only 0:20 h on the same machine and is thus significantly faster.

In Fig. 2a, the simulated gain over the frequency is shown for a 1 W input signal. A maximal gain of roughly 35 dB is simulated by both simulation tools. The frequency dependency and the simulated 3 dB bandwidth of 7.5 GHz is in a good agreement between the both simulation tools. However, the gain curve simulated by the method presented here is shifted towards higher frequencies by about 0.75 GHz. In addition, the gain simulated with simpleRick drops faster for frequencies below 87 GHz. The reason for the differences at low frequencies is the utilized coupled modes method. Especially for lower frequencies, the inaccuracies of the coupled modes equations increase because the coupled $\mathrm{TE}_{1,1}$ mode is assumed to be non-dispersive at the investigated frequencies (see (10)). Therefore, the approximated dispersion relation differs slightly from the real dispersion which influences the beam-wave interaction.

B. Sub-THz Helical Gyro-TWT

The helically corrugated interaction region of the sub-THz gyro-TWT has a mean radius of $R = 0.528\,\mathrm{mm}$ with a corrugation of $\tilde{r} = 0.08\,\mathrm{mm}$ and $\tilde{d} = 1.11\,\mathrm{mm}$ at a total length of $L = 35\,\tilde{d}$. It is operated with a 0.4 A electron beam with a beam voltage of $U_\mathrm{b} = 40\,\mathrm{kV}$ and a pitch factor of $\alpha = 1.0$ at a constant magnetic field of 5.015 T.

A similar spacial discretization as in the previous example is used which results in $2 \cdot 10^6$ mesh cells for the CST model. For both simulation tools, a time step of $dt = 0.05\,\mathrm{ps}$ is used and the electron beam is modeled by $100 \cdot 10^3$ macro particles. A spatial discretization of $dx = dy = 0.025\lambda$ in the transversal dimension and $dz = 0.03\lambda$ in the longitudinal dimension is used for the CST MS simulation setup which results in $4 \cdot 10^6$ mesh cells.

While the simulation with CST MS takes 9:30 h on the utilized computer, the simulation with the method presented in this paper requires only 0:35 h. Therefore, in both examples, W-band and sub-THz helical gyro-TWT, a speed-up of about 16 is observed.

In Fig. 2b, the corresponding simulated gain curves are shown. The curves are in good agreement between both simulation models. The new simulation model predicts a slightly higher gain than CST MS (+0.5 dB) and again a slight shift of the gain curve by 1 GHz towards higher frequencies is observed. However, the overall shape of the curves are in a great agreement.

V. Conclusion

The presented approach for the simulation of gyro-TWTs with HCIR is a link between classical methods with slowly varying values approaches and full-wave PIC solvers. The basic equations as well as the numerical solution of the new hybrid model were presented and the new developed model was validated against the commercial full-wave PIC solver CST MS. A good agreement between the simulation results is observed while the computing time is significantly reduced.

The new approach is in particular well suited for the initial design process of a tube and automated synthesis/optimization procedures where a high number of simulations is required.

If more detailed investigations are required, further effects can easily be added to the model. For example, space-charge effects can be added if an additional space-charge field is

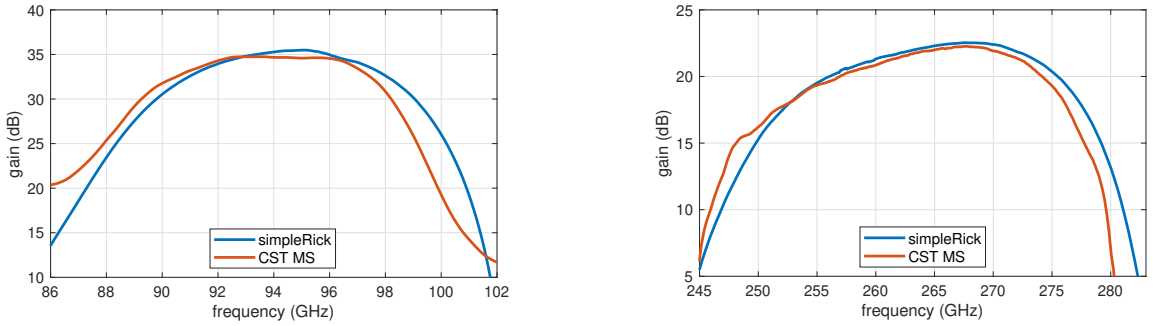

(a) (b)

Fig. 2. Comparison of the frequency dependent saturated gain simulated with CST MS and simpleRick. (a) For a W-band helical gyro-TWT; (b) For a sub-THz helical gyro-TWT.

calculated in each particle pushing step, e.g. using the method presented in [28]. Therefore, advanced effects can also be studied with the proposed model. The advantage is that the influences of all these effects can be well separated and individually investigated, which is often difficult in full-wave PIC approaches.

However, each additional extension of the model slows down the simulations and beyond a certain threshold, using a highly optimized commercial full-wave PIC solver such as CST MS will become faster. Furthermore, if an HCIR with a strong corrugation ($\tilde{r} > \lambda/10$) is investigated, the coupled modes approach loses its validity and again a full-wave PIC solver is the appropriate choice. In future, this limitation can be addressed if the circular waveguide eigenmodes would be replaced by numerically calculated eigenmodes of the HCIR. The advantage of the proposed PIC approach is, that the particle handling and the source term calculation will work also with numerically calculated eigenmodes without any changes.

Finally, a full-wave PIC solver is also the appropriate choice for the final verification of a newly developed design.

References

[1] T. V. Can, J. J. Walish, T. M. Swager, and R. G. Griffin, "Time domain DNP with the NOVEL sequence," *J. Chem. Phys.*, vol. 143, no. 5, p. 054 201, 2015. DOI: 10.1063/1.4927087.

[2] K. O. Tan, C. Yang, R. T. Weber, G. Mathies, and R. G. Griffin, "Time-optimized pulsed dynamic nuclear polarization," *Sci. Adv.*, vol. 5, no. 1, eaav6909, 2019. DOI: 10.1126/sciadv.aav6909.

[3] G. G. Denisov, V. L. Bratman, A. D. Phelps, and S. V. Samsonov, "Gyro-TWT with a helical operating waveguide: New possibilities to enhance efficiency and frequency bandwidth," *IEEE Trans. Plasma Sci.*, vol. 26, no. 3, pp. 508–518, Jun. 1998. DOI: 10.1109/27.700785.

[4] N. S. Ginzburg, S. V. Samsonov, G. G. Denisov, *et al.*, "Ka-band 100-kW subnanosecond pulse generator mode-locked by a nonlinear cyclotron resonance absorber," *Phys. Rev. Applied*, vol. 16, p. 054 045, 5 Nov. 2021. DOI: 10.1103/PhysRevApplied.16.054045.

[5] Dassault Systèmes, *CST studio suite - electromagnetic field simulation software*, version 2020, Jun. 13, 2020. [Online]. Available: https://www.cst.com.

[6] B. Goplen, L. Ludeking, D. Smith, and G. Warren, "User-configurable MAGIC for electromagnetic PIC calculations," *Comput. Phys. Commun.*, vol. 87, no. 1-2, pp. 54–86, 1995. DOI: 10.1016/0010-4655(95)00010-D.

[7] S. Kern, "Numerische Simulation der Gyrotron-Wechselwirkung in koaxialen Resonatoren," German, 31.04.02; LK 01; Karlsruhe 1996. (Wissenschaftliche Berichte. FZKA. 5837.) Fak. f. Elektrotechnik, Diss. v. 12.7.1996., Ph.D. dissertation, 1996. DOI: 10.5445/IR/55396.

[8] M. Botton, T. Antonsen, B. Levush, K. Nguyen, and A. Vlasov, "Magy: A time-dependent code for simulation of slow and fast microwave sources," *IEEE Plasma Sci.*, vol. 26, no. 3, pp. 882–892, 1998. DOI: 10.1109/27.700860.

[9] K. A. Avramides, I. G. Pagonakis, C. T. Iatrou, and J. L. Vomvoridis, "Euridice: A code-package for gyrotron interaction simulations and cavity design," in *EPJ Web of Conferences*, EDP Sciences, vol. 32, 2012, p. 04 016. DOI: 10.1051/epjconf/20123204016.

[10] F. Braunmueller, T. M. Tran, Q. Vuillemin, *et al.*, "TWANG-PIC, a novel gyro-averaged one-dimensional particle-in-cell code for interpretation of gyrotron experiments," *Phys. Plasmas*, vol. 22, no. 6, p. 063 115, 2015. DOI: 10.1063/1.4923299.

[11] C. Wu, K. A. Avramidis, M. Thumm, and J. Jelonnek, "An improved broadband boundary condition for the RF field in gyrotron interaction modeling," *IEEE Trans. Microw. Theory Tech.*, vol. 63, no. 8, pp. 2459–2467, 2015. DOI: 10.1109/TMTT.2015.2433270.

[12] A. Sawant and E. Choi, "Development of the full package of gyrotron simulation code," *J. Korean Phys. Soc.*, vol. 73, no. 11, pp. 1750–1759, 2018, ISSN: 1976-8524. DOI: 10.3938/jkps.73.1750.

[13] P. Wang, X. Chen, H. Xiao, O. Dumbrajs, X. Qi, and L. Li, "Gyrocompu: Toolbox designed for the analysis of

gyrotron resonators," *IEEE Plasma Sci.*, vol. 48, no. 9, pp. 3007–3016, 2020. DOI: 10.1109/TPS.2020.3013299.

[14] G. G. Denisov and M. G. Reznikov, "Corrugated cylindrical resonators for short-wavelength relativistic microwave oscillators," *Radiophysics and Quantum Electronics*, vol. 25, no. 5, pp. 407–413, 1982, ISSN: 1573-9120. DOI: 10.1007/BF01035315.

[15] S. Cooke and G. Denisov, "Linear theory of a wideband gyro-TWT amplifier using spiral waveguide," *IEEE Plasma Sci.*, vol. 26, no. 3, pp. 519–530, 1998. DOI: 10.1109/27.700786.

[16] S. Zhu, E. Wang, H. Li, H. Li, and J. Feng, "Self-consistent nonlinear theory and simulation of gyro-twt with helically corrugated waveguide," *IEEE Plasma Sci.*, vol. 40, no. 2, pp. 443–450, 2012. DOI: 10.1109/TPS.2011.2174657.

[17] N. S. Ginzburg, I. V. Zotova, A. S. Sergeev, *et al.*, "Mechanisms of amplification of ultrashort electromagnetic pulses in gyrotron traveling wave tube with helically corrugated waveguide," *Phys. Plasmas*, vol. 22, no. 11, p. 113 111, 2015. DOI: 10.1063/1.4935905.

[18] N. S. Ginzburg, G. S. Nusinovich, and N. A. Zavolsky, "Theory of non-stationary processes in gyrotrons with low Q resonators," *Int. J. Electron.*, vol. 61, no. 6, pp. 881–894, 1986. DOI: 10.1080/00207218608920927.

[19] N. Marcuvitz, Ed., *Waveguide handbook* (Radiation Laboratory series 10), 1. ed. New York [u.a.]: McGraw-Hill, 1951.

[20] A. W. Fliflet, M. E. Read, K. R. Chu, and R. Seeley, "A self-consistent field theory for gyrotron oscillators: Application to a low Q gyromonotron," *Int. J. Electron.*, vol. 53, no. 6, pp. 505–521, 1982. DOI: 10.1080/00207218208901545.

[21] J. Crank and P. Nicolson, "A practical method for numerical evaluation of solutions of partial differential equations of the heat-conduction type," *Adv. Comput. Math*, vol. 6, no. 1, pp. 207–226, 1996, ISSN: 1572-9044. DOI: 10.1007/BF02127704.

[22] F. Jeanette, *Intel math kernel library. reference manual*, 2016.

[23] C. S. Peskin, "The immersed boundary method," *Acta Numerica*, vol. 11, p. 479 517, 2002. DOI: 10.1017/S0962492902000077.

[24] J. M. Dawson, "Particle simulation of plasmas," *Rev. Mod. Phys.*, vol. 55, pp. 403–447, 2 Apr. 1983. DOI: 10.1103/RevModPhys.55.403.

[25] C. Runge, "Ueber die numerische Aufloesung von Differentialgleichungen," *Math. Ann.*, vol. 46, no. 2, pp. 167–178, 1895, ISSN: 1432-1807.

[26] J. P. Boris, "Relativistic plasma simulation-optimization of a hybrid code," in *Proc. Fourth Conf. Num. Sim. Plasmas*, 1970, pp. 3–67.

[27] S. Samsonov, A. Bogdashov, I. Gachev, and G. Denisov, "Studies of a gyrotron traveling-wave tube with helically corrugated waveguides at IAP RAS: Results and prospects," *Radiophys. Quantum Electron.*, vol. 62, no. 7, pp. 455–466, Mar. 2020. DOI: 10.1007/s11141-020-09991-1.

[28] J. Qiang and R. D. Ryne, "Parallel 3d poisson solver for a charged beam in a conducting pipe," *Comput. Phys. Commun.*, vol. 138, no. 1, pp. 18–28, 2001, ISSN: 0010-4655. DOI: https://doi.org/10.1016/S0010-4655(01)00185-0.